TBME-01137-2023.R2

Prosthetic Limb Attachment via Electromagnetic Attraction through a Closed Skin Envelope

Will Flanagan, Kai Becraft, Haley Warren, Alexandra I. Stavrakis, Nicholas M. Bernthal, Thomas J. Hardin, and Tyler R. Clites*

Abstract— Objective: Current socket-based methods of prosthetic limb attachment are responsible for many of the dominant problems reported by persons with amputation. In this work, we introduce a new paradigm for attachment via electromagnetic attraction between a bone-anchored ferromagnetic implant and an external electromagnet. Our objective was to develop a design framework for electromagnetic attachment, and to evaluate this framework in the context of transfemoral amputation. **Methods:** We first used inverse dynamics to calculate the forces required to suspend a knee-ankle-foot prosthesis during gait. We then conducted cadaveric dissections to inform implant geometry and design a surgical methodology for covering the implant. We also developed an *in silico* framework to investigate how electromagnet design affects system performance. Simulations were validated against benchtop testing of a custom-built electromagnet. **Results:** The physical electromagnet matched simulations, with a root-mean-square percentage error of 4.2% between measured and predicted forces. Using this electromagnet, we estimate that suspension of a prosthesis during gait would require 33 W of average power. After 200 and 1000 steps of simulated walking, the temperature at the skin would increase 2.3℃ and 15.4℃ relative to ambient, respectively. **Conclusion:** Our design framework produced an implant and electromagnet that could feasibly suspend a knee-ankle-foot prosthesis during short walking bouts. Future work will focus on optimization of this system to reduce heating during longer bouts. **Significance:** This work demonstrates the initial feasibility of an electromagnetic prosthetic attachment paradigm that has the potential to increase comfort and improve residual limb health for persons with amputation.

***Index Terms*— prosthetic limb attachment, surgical implants, electromagnetics, anatomics**

I. INTRODUCTION

Recent efforts in prosthetic research have focused on creating robotic devices that are closer than ever to replicating the capabilities of their biological counterparts [1]–[11]. For persons with amputation, however, problems related to the mechanical attachment of these devices to the body impact quality of life at least as much as functional deficiencies of the limbs themselves [12]–[14]. Current attachment methods cause excessive heat and sweating, tissue damage, and residual limb pain. This contributes to most patients being dissatisfied with their prosthetic care [12] and high prosthesis abandonment rates [15], even with advanced devices [16]. Preserving residual limb health is costly: each patient on average visits their prosthetist 7-9 times per year [13], [17], and the average annual cost of prosthesis-related care for a patient with above-knee amputation is $5-10K [17], [18]. Due to disparities in access to healthcare and other resources, these issues disproportionately affect people from underprivileged socioeconomic communities and racial minorities, who are up to four times more likely to undergo preventable amputations [19].

In all current socket-based systems, the loads required to hold the prosthesis onto the body are borne by the skin, muscle, and fat of the residual limb, rather than by the bone. These loads are typically transferred to the residuum via friction or suction between the socket (or liner) and the skin. Because soft tissues deform under load, each loading cycle causes these tissues to stretch and compress about the residual bone. This relative motion between the socket and the bone is known as “pistoning". Pistoning is a dangerous phenomenon that leads to tissue breakdown, skin ulcers, and poor prosthetic control [20]. This is especially a concern considering that amputations are frequently performed in patients with medical comorbidities, such as peripheral artery disease, that already elevate the risk of wounds and infection [21]. Current strategies to reduce pistoning emphasize distributing socket forces across a greater surface area [22], with a goal of reducing soft tissue deformation. Unfortunately, this has led to sockets that enclose large portions of the residual limb in non-breathable materials, creating the hot, damp environments that exacerbate skin problems [23]. Although newer technologies such as vacuum suspension [24] and high-fi sockets [25] have shown improvements over pin-lock or lanyard-based sockets, these systems have been unable to overcome the comfort and pistoning challenges inherent to soft-tissue suspension.

The problems with soft tissue attachment are severe enough that some patients opt for percutaneous osseointegration (OI), a surgically invasive attachment method wherein the prosthesis is connected directly to the residual bone via a metal implant protruding *through* the skin. For patients eligible for the procedure, OI has provided significant improvements to clinical outcomes, quality of life, prosthetic use, and prosthetic embodiment [26]–[28]. Patients with OI also report satisfaction with devices commonly described as “too heavy”, suggesting a higher tolerance of prosthetic mass when suspending from bone [28]–[30]. The primary barrier for

This work was supported in part by the National Science Foundation Graduate Research Fellowship Program under Grant DGE-2034835, in part by the U.S. Department of Defense under Grant W81XWH2220046, and in part by the National Science Foundation Disability and Rehabilitation Engineering Program under Grant 2144015.

W. Flanagan, K. Becraft, and H. Warren are with the Department of Mechanical and Aerospace Engineering, University of California, Los Angeles.

A. I. Stavrakis and N. M. Bernthal are with the Orthopaedic Hospital Research Center, Orthopaedic Hospital Department of Orthopaedic Surgery, and David Geffen School of Medicine, University of California Los Angeles.

T. J. Hardin is with the Material, Physical, and Chemical Sciences Center, Sandia National Laboratories 87123 USA.

*T. R. Clites is with the Departments of Mechanical and Aerospace Engineering and Orthopaedic Surgery, University of California Los Angeles. (correspondence email: clites@ucla.edu)

adoption of OI is that it requires a chronically perforated skin envelope. This creates a substantial infection risk [31]–[36], contributing to an overall implant failure rate of around 20% [36]–[39]. Additionally, OI surgery and the resultant chronic wound place an elevated healing load on the body, which limits applicability of the approach in persons with compromised healing ability. This typically precludes OI in cases of dysvascular amputation, which accounts for 77% of major limb amputation [21].

In response to these challenges, we introduce a new socket suspension paradigm that transfers suspension loads directly from the prosthesis to residual bone, while maintaining a sealed skin envelope. Our system has two core components: a subcutaneous ferromagnetic implant in the residual bone, and an electromagnet in the distal end of the socket. These components allow us to engineer both the body and machine in parallel in pursuit of greater function. When current flows through the electromagnet, an *attractive* force is produced between the magnet and the implant, along the residual bone's primary load-bearing axis. The magnitude of this attractive force can be directly controlled by modulating the electrical current through the electromagnet's coils. Note that this approach is intended to generate *attractive* forces rather than *repulsive* forces. During weightbearing, compressive stresses would be transmitted to the soft tissues as in conventional sockets, albeit with the benefits of the implant's larger distal surface area compared to the residual bone [40], [41]. Although magnetic repulsion could be used to off-load these compressive stresses, any strategy built around "repulsive levitation" would require implanting a permanent magnet into the residual limb. An implanted permanent magnet strong enough to levitate a person would also be strong enough to cause significant harm in the presence of external ferromagnetic material (e.g. the refrigerator door) by generating hundreds of pounds of attractive force that could crush tissues surrounding the implant.

This manuscript details a design framework by which electromagnetic attachment systems can be developed for any amputation level. As a test case, we validated this framework in the context of transfemoral amputation. Our goal was to assess the feasibility of electromagnetic suspension, and to understand how electromagnet design influences system performance.

Our design framework begins with *biomechanical analysis*, in which we model the expected use case (in our case level-ground walking) to characterize the socket forces transferred to the residuum. We use those data to inform *implant design*, which involves cadaveric dissections to determine implant size and shape. In parallel, we carry out our *electromagnet design* process in simulation to balance force requirements with other design priorities (e.g. mass, power). In this study, we validated the feasibility of the design produced by this framework on the benchtop by investigating power requirements (*power feasibility*) and heating (*thermal feasibility*). This manuscript concludes with an exploration of how this framework could be used to optimize application-specific electromagnets in the context of different design priorities (*cost function analysis*).

II. Methods

A. System overview

The proposed magnetic attachment system transfers suspension loads from a prosthetic limb directly to the residual bone via magnetic attraction (**Fig. 1a**). An external electromagnet housed in the socket actively modulates the attractive force (F_{mag}) between itself and a subcutaneous bone-anchored ferromagnetic implant to suspend the prosthesis.

B. Biomechanical analysis

To estimate the socket pulloff force (F_p) required to suspend a prosthesis during gait, we first modified a 23 degree-of-freedom (DOF) skeletal model (**Fig. 1b**) to simulate a mid-femur transfemoral amputation. The length, mass, and inertia of the affected femur was scaled so that the modified femur was half as long. A rigid "joint" was added along the long axis of the modified femur, with an origin at the modified femur's distal end, to simulate the limb-socket interface. This joint was connected to the original knee joint by a "socket" body. The socket was modeled as a cylinder of length equal to the original femur and mass of 1 kg, which was chosen to approximate an average socket. The masses of the affected tibia (4.7 kg) and foot (0.53 kg) were set to model a heavy powered knee-ankle-foot prosthesis [42], and inertias were scaled accordingly.

We used biomechanical data from 5 subjects of the Hood et al. dataset [43] with our model and re-computed the inverse

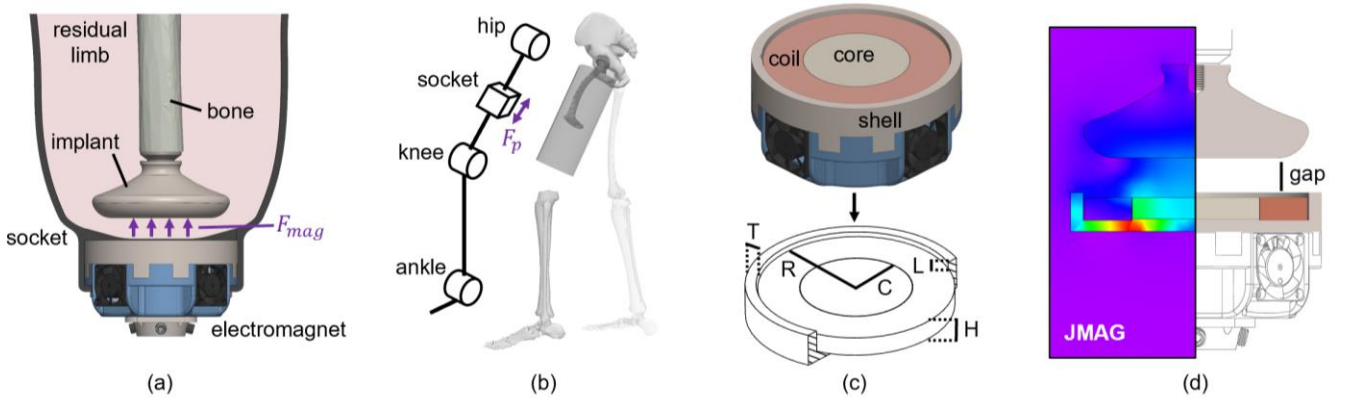

Figure 1. Electromagnetic attachment system for prosthetic limbs. (a) The system is composed of a bone-anchored implant inside the residual limb and an external electromagnet housed within the socket. (b) The pulloff force (F_p) during gait was estimated using a musculoskeletal model in OpenSim. (c) The electromagnet consists of a core surrounded by coils and enclosed in a ferromagnetic shell. This geometry was parametrized by the core radius (C), core/coil height (H), coil radius (R), shell thickness (T), and lip height (L). (d) The system was simulated in the software JMAG using the implant positioned above the parametrized electromagnet separated by the nominal gap distance.

dynamics pipeline in OpenSim [44]. A sample size of 5 was deemed appropriate for this analysis because it brought our 95% confidence interval on the margin of error in peak pulloff force to below 10% of the peak magnitude. The subjects were chosen at random from [43], and provided a large range of both height (1.65-1.91 m) and body mass (58.5-104.3 kg). Only trials for level-ground walking at 0.8 m/s were considered, because this was closest to the average self-selected walking speed of the patient population [45]. Socket pulloff force was extracted from the inverse dynamics results as the force on the socket joint in the direction of the femur's long axis. All individual-step trajectories were averaged for each of the 5 subjects to produce 5 subject-specific pulloff force trajectories. To determine how the addition of the electromagnet would affect F_p, we repeated these analyses for socket masses of 1.25, 1.5, 1.75, and 2 kg, corresponding to electromagnet masses of 0.25-1.0 kg.

C. Implant design

The implant is designed to affix to the distal end of the residual femur (Fig. 1a) via a modular attachment that could mate with existing third-party cementless stems. The implant is composed of ferritic stainless steel (SS420), coated in non-magnetic titanium-nitride (TiN) for enhanced biocompatibility. To determine a suitable implant geometry, we simulated a mid-length transfemoral amputation in two cadavers. All cadaver work was done under an approved protocol from the UCLA Donated Body Program (#107039) and the USAMRDC Office of Human Research Oversight (E03736.1a). Based on these dissections, we sized the implant to fit within the limb, and generated a shape that would maximize the amount of material at the distal end, to increase magnetic attraction. To limit the risk of implant extrusion or tissue breakdown, we had three key design priorities: i.) all edges of the implant must be rounded to limit stress concentrations in the surrounding tissues, ii.) the profile of implant needed to be entirely convex, to avoid any possibility of dead space, and iii.) the implant must be fully covered by muscle, tendon, or fascia, which can withstand prolonged loaded contact with synthetic materials. Once we had identified a potential coverage strategy, we measured the tissue thickness between the distal surface of the implant and the surface of the skin, to determine the gap distance that would exist between the electromagnet and the implant.

D. Electromagnet design

The generic electromagnet design for our simulation framework is composed of a permanent magnet core (NdFeB) surrounded by a copper coil, all within a SS420 shell (**Fig. 1c**). We parametrized this design by the core radius (C), coil radius (R), shell thickness (T), coil/core height (H), and shell lip height (L). These parameters were bounded on the upper end to ensure that the electromagnet would fit within a prosthetic socket, and on the lower end to ignore electromagnets that would be far too weak to suspend a prosthesis (**Table 1**).

The system was simulated using static 3D magnetic field analysis in the software JMAG (JSOL Corporation, Tokyo Japan). In these simulations, the implant was positioned above the electromagnet and separated by the expected gap distance (**Fig. 1d**). The space between the implant and electromagnet was modeled as an air gap because all materials in the gap (i.e. biological tissue, TiN implant coating, socket liners) have magnetic permeabilities close to that of air. The result of each simulation was the net magnetic force on the implant (F_{mag}).

For a given electromagnet geometry, we calculated the number of turns in the coil (N) as:

$$N = \frac{0.9 * A_{coil}}{A_{wire}}; \qquad A_{coil} = H * (R - C)$$

where A_{coil} is the coil cross-sectional area, 0.9 is the fill factor for orthocyclic windings, and A_{wire} is the cross-sectional area of a nominal wire size (18 awg). Depending on the goals of a given simulation, coil current (I) was either set to a desired current, or calculated to correspond to a desired electrical power; in these calculations, we assumed that the coil's inductance was small, such that only resistive heating occurred ($P = I^2R$). The resistance was calculated by multiplying the resistance per unit length of a nominal wire gauge by the wire length. Wire length (l_w) was determined by estimating the copper volume as the fill factor times the coil volume (V_{coil}), then dividing this volume by the wire cross-sectional area:

$$l_w = \frac{0.9 * V_{coil}}{A_{wire}}; \quad V_{coil} = H * \frac{\pi}{4}(R^2 - C^2)$$

Each electromagnet design was evaluated based on the peak power (P_{max}) required during gait, the electromagnet mass (M_{mag}), and the attractive force at a nominal gap distance with zero current through the coils (i.e. the force created by the permanent magnet core). We refer to this last metric as the *zero-current force* (F_0). For an electromagnet design, M_{mag} was calculated based on each material's volume and density. To determine P_{max}, the peak pulloff force during gait ($F_{p,max}$) was found using the relationship between the inter-subject average $F_{p,max}$ and M_{mag} from our biomechanical analyses. The current required to reach $F_{p,max}$ was calculated using the relationship between F_{mag} and I from JMAG simulations and converted to power using $P = I^2R$. The zero-current force (F_0) was defined as F_{mag} at a gap distance of 17.5 mm when $I = 0\ A$.

Our objective was to find an electromagnet design with P_{max} less than 300 W, M_{mag} around 1 kg, and F_0 around 50 N. We set the P_{max} limit at 300 W so that our device would have a similar peak power to current prosthetic limbs, which allows us to use similar power electronics. The M_{mag} limit was used to restrict the mass that would be added to the socket. The F_0 specification was set to the max value that would still allow for the magnetic field from the coils to cancel out the permanent magnet core at a reasonable current. In other words, we wanted to ensure that our system could be "shut off", to facilitate removal of the prosthesis (doffing) or if something magnetic was dropped into the socket. Limiting F_0 also reduces the added compressive force the magnet exerts on the limb during stance.

To understand how the core material (NdFeB grade) and each of the geometric parameters affect these performance metrics, we performed a one-dimensional parameter sweep about an initial design. This initial design represents a geometry—found through random sampling—that came close to meeting our design specifications, and served as a central point about which we explored the local effects of isolated changes to each parameter. For each parameter, we selected a design range and evaluated the performance of electromagnets

with the parameter of interest varying within that range, and all other parameters equal to the initial design values. The influence of each parameter was determined by the range of the performance metric resulting from varying the design parameter over its design range.

Having understood the effects of each design parameter, we manually iterated through combinations of these parameters in simulation to find a geometry and core material that met our design specifications. As we finalized the electromagnet design for manufacturing, we came across two design decisions that did not directly affect performance according to our metrics, but would impact the feasibility of the final system. Specifically, the interplay between coil wire size and battery voltage does not impact P_{max}, but does set the max force that the electromagnet can produce. Although the force produced by for a given *power* is independent of wire size, the force produced for a given *voltage* is directly tied to the wire size, which determines the coil's resistance and the number of turns that fit within a given volume. Maximum possible attractive force is achieved when the full battery voltage is applied to the electromagnet in the positive direction. We wanted this system to have a factor of safety at least 1.5 times the inter-subject average $F_{p,max}$ (i.e. the peak pulloff force seen during gait), to ensure the limb remains attached in cases of excess loading. This factor of safety corresponds to 4 standard deviations above $F_{p,max}$ based on our biomechanical analyses. Additionally, applying the full battery voltage in the negative direction (coil's magnetic field opposing the permanent magnet core) determines how much the force can be lowered below F_0. This is useful as a safety mechanism or in the case of prosthesis doffing. We desired this "doffing" force (F_{doff}) to be below 10 N. As a final consideration, the current when the full battery voltage is applied should be within the peak current capabilities of the driver such that the system can be controlled over the full force range. Drive electronics in powered prostheses have a peak current near 30 A [42].

To select a battery voltage and wire size that would meet these criteria, we simulated the system at full positive and negative voltages for 24, 36, and 48 V batteries and wire sizes of 15-24 awg, and recorded the electromagnet current and attractive force on the implant for each case. We then made modifications to the electromagnet geometry to enforce an integer number of layers in the coil and manufacturer-specific clearances. Additional components around the electromagnet were then designed to complete the system, such as a spacer between the electromagnet and the skin, a liner above this spacer, a heat sink below the electromagnet, an aluminum housing, and cooling fans. The spacer is a cup-shaped plastic ring used to form the top of the electromagnet to resemble the bottom of a socket. This also thermally insulates the limb from the electromagnet coils. A 2.5 mm thick silicone sheet simulating a prosthetic liner was mounted on the spacer.

E. Power feasibility

To evaluate electromagnetic attachment at the transfemoral level, we investigated the power required to suspend a prosthesis during gait, and the heating that would occur from continuous walking. We first validated the JMAG simulations by characterizing the manufactured system on the benchtop. The implant was mounted to a linear stage opposite the electromagnet, which was mounted on a fixed support, such that the gap distance between the implant and electromagnet could be set. A uniaxial load cell between the implant and linear stage measured the force applied to the implant (F_{mag}). The electromagnet current (I) was controlled via a servocontroller (ESCON 70/10, Maxon Inc.). At several gap distances, we measured F_{mag} as a function of I, and compared our results to the JMAG simulations via root-mean-square percentage error.

Using a quadratic fit between the measured F_{mag} and I data at the nominal gap distance, we calculated the current required to produce the step-by-step pulloff force for each subject from our biomechanical analyses. Points in the gait cycle with negative currents (i.e., the coil's field counteracts that of the core) were set to zero, such that the electromagnet is "off" at these times. During stance, the zero current force of the permanent magnet core would increase compressive forces on the residual limb, however, an F_0 of 50 N would only increase peak weightbearing force by at most 10%, based on our biomechanical analyses. The resulting current profiles were converted to instantaneous power using the coil resistance of the manufactured electromagnet. Computing power in this way assumed the system was quasi-static, which is acceptable given that the electromagnet's low inductance reduces this system to 0^{th} order dynamics on the time scale of a gait cycle. The average power for each subject was found by integrating the instantaneous power profile and dividing by mean stride time.

F. Thermal feasibility

Heating during continuous walking was evaluated on the testbench by recording temperatures of the system as current was repeatedly driven through the electromagnet. To simplify the current profile while maintaining the time-dynamics of the system, we discretized the inter-subject instantaneous power curve into 6 bins based on the profile's characteristics (peaks/valleys). The power for each bin was set to the average power for that time interval. This power was converted to the desired electromagnet current using $I = \sqrt{P/R}$.

To simulate the residual limb, we molded a mock distal end of the limb out of a silicone elastomer (Ecoflex 00-31, Smooth-On Inc.) around the implant. The thickness of the silicone distal to the implant was set to 15 mm thick, such that the total gap distance was the nominal 17.5 mm after accounting for the 2.5 mm thick silicone sheet from the liner between the electromagnet and the skin. Surface temperatures at several locations on the magnet and liner were measured using a smartphone-based thermal scanner (ONE Pro, FLIR Systems), as the current profile over gait was replayed for 500 strides (1000 steps). Tape (Scotch Super 88, 3M) was affixed to the measurement locations to control surface emissivity ($\varepsilon = 0.95$) [46]. The two sets of trials run for a single condition (passive or active cooling) consisted of the limb in contact with the liner, with the temperatures of the shell and housing measured from the side, along with a separate trial without the limb such that the temperature of the liner could be measured. 5 trials of each setup (with/without the residuum) were performed for the electromagnet being passively (fans off) and actively (fans on) cooled for a total of 20 trials. The ambient temperature (23°C) was measured throughout each trial and the electromagnet was allowed to cool to ambient between each trial.

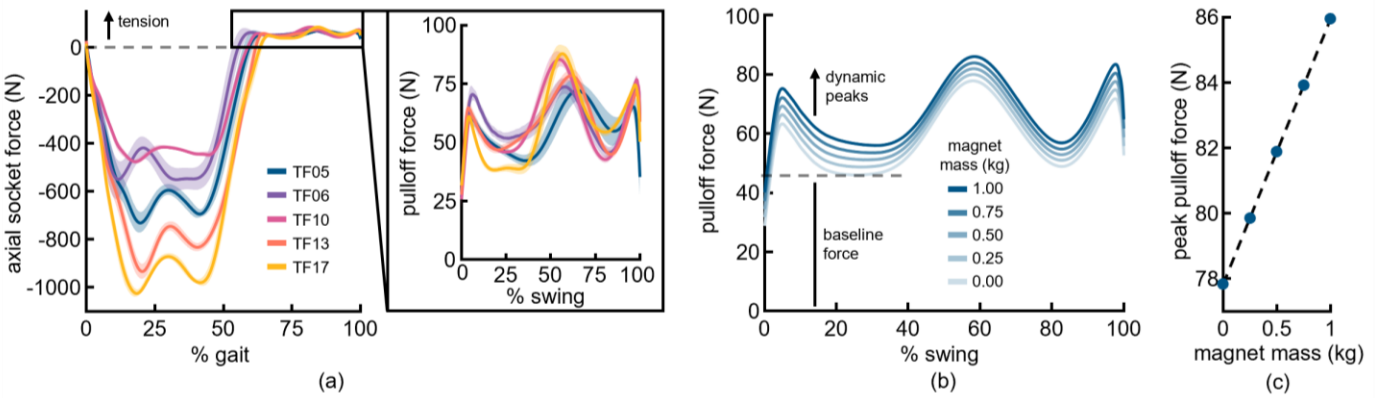

Figure 2. Socket force during gait for five persons with transfemoral (TF) amputation generated using biomechanical data from [43]. (a) Axial socket forces for the full gait cycle and isolated swing phase (detail view). Shaded regions show ±1 st. dev. (b) Inter-subject average pulloff force during swing for varying electromagnet mass. The "baseline" force is the lower bound of the force profile, and "dynamic peaks" are the transient force increases to this baseline. (c) Peak pulloff force as a function of electromagnet mass. In all plots, positive forces denote tension.

G. Cost function analysis

Our objective in benchtop testing one electromagnet was to validate our design framework and study initial feasibility of electromagnetic attachment. In the future, this framework will facilitate optimization of the electromagnet. To this end, we propose a cost function to be minimized based on the force at 300 W power (F_{300}), the peak pulloff force ($F_{p,max}$), the electromagnet mass (M_{mag}), and the zero-current force (F_0):

$$J = C_f\left(F_{p,max} - F_{300}\right) + C_m\left(9.81 * M_{mag}\right) + C_0 F_0$$

The cost weights for this cost function (C_f, C_m, C_0) can be varied based on the relative importance of power, mass, and zero-current force for a specific application. We sought to understand this optimization landscape by investigating how these weights would affect the geometry of the optimal (minimum cost) design. We sampled the design space of C, H, R, and T through a 4-dimensional grid sweep, containing 4356 unique combinations of the 4 parameters. For all designs the lip height (L) was held constant at 2.5 mm and the permanent magnet core was grade n42. M_{mag}, $F_{p,max}$, F_0, and F_{300} were calculated in JMAG for each combination of parameters. The weights C_f and C_m were varied between 10^{-2} and 10^2 in a 2-dimensional sweep, with C_0 set to unity; because there is no absolute cost scale, only relative values of the weights are important in guiding the optimization. The effect of changing C_0 could still be studied by dividing by $C_f C_m$ for points where $C_f = C_m$. For each set of cost weights, the costs for all sampled electromagnet geometries were calculated and the geometry with the lowest cost was recorded as the optimal geometry for that set of weights. We used this mapping of cost weights to optimal geometry to investigate how the optimal value of each parameter was affected by the relative importance of each design priority. From this mapping, we selected three "optimal" designs: one prioritized power, one prioritized mass, and one prioritized zero current force. For each optimal design, we evaluated the average power during gait (P_{avg}) and the power required to reach the desired 10 N doffing force (P_{doff}).

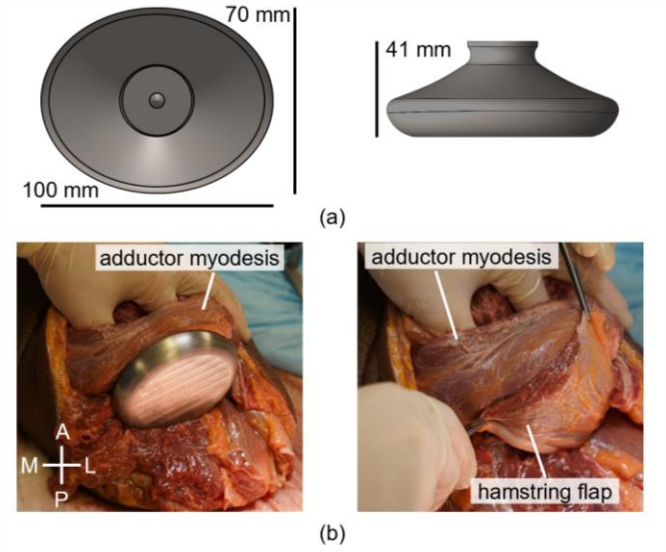

Figure 3. Surgical design, as informed by cadaveric dissections. (a) The implant is ovular in shape with a large distal end and rounded edges. (b) The implant will be fully covered using a hamstring flap (biceps femoris and semimembranosus) and adductor myodesis.

III. Results

A. Biomechanical analysis

Our inverse dynamics analysis showed that weightbearing forces vary greatly across subjects during stance. In contrast, pulloff forces during swing are similar in both magnitude and timing across subjects (**Fig. 2a**): the mean inter-subject standard deviation over swing was 6.1 N. Tensile forces during swing had much lower magnitudes than compressive forces during stance. During swing, the pulloff force can be split into a "baseline" force, corresponding to the static mass of the system, and three dynamic force peaks, related to limb motion (**Fig. 2b**).

Increasing electromagnet mass linearly increased peak pulloff forces during swing:

$$F_{p,max} = 8.12\ \frac{N}{kg} * M_{mag} + 77.8\ N$$

The offset term corresponds to the peak suspension force required for the socket and prosthesis, independent of the magnet. For a 1 kg electromagnet, $F_{p,max}$ was 86 N. The baseline force during swing for this mass was 55 N.

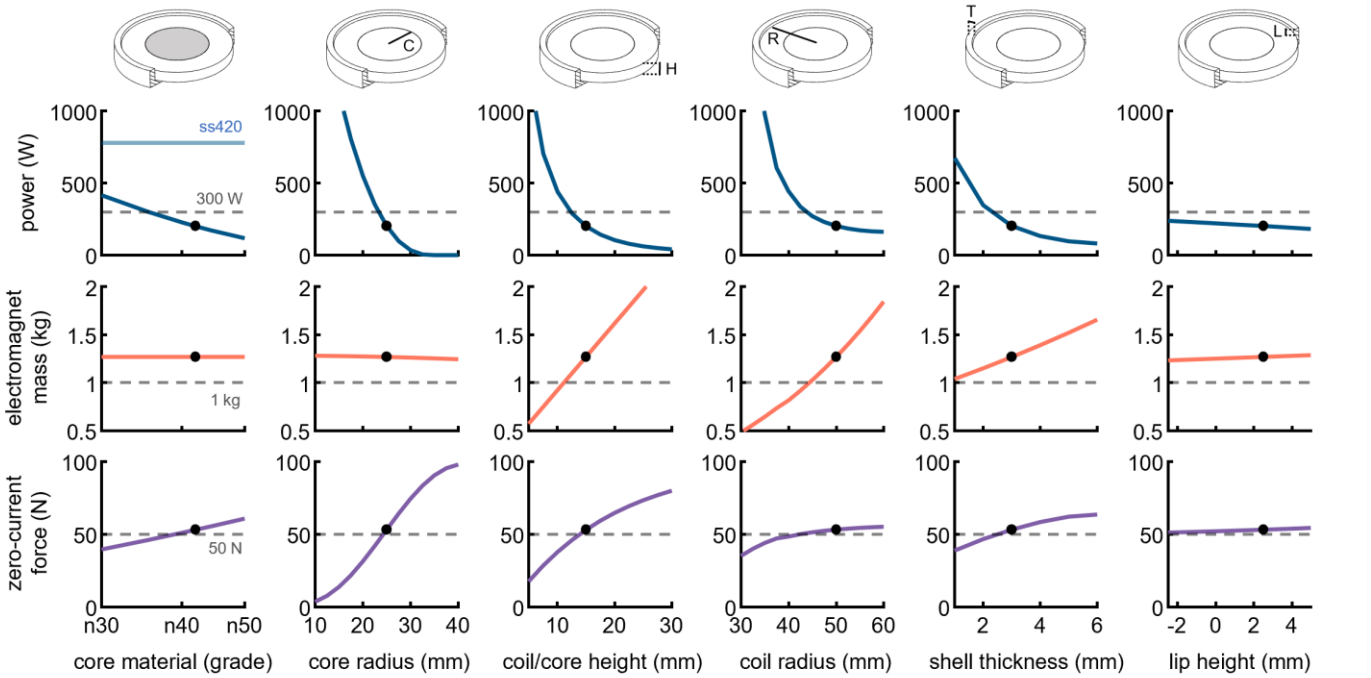

Figure 4. Effect of design parameters on peak power during gait, electromagnet mass, and zero-current force. The peak power is the power required to produce the peak pulloff force during gait for the corresponding electromagnet mass. The zero-current force is the force on the implant when no current is applied to the electromagnet, at the nominal 17.5 mm gap distance. Each design parameter was independently swept while all other parameters remained constant at an initial design (denoted by the marker). Dashed lines on each plot represent the design specifications, with feasibility targets for peak power set at less than 300 W, electromagnet mass at around 1 kg, and zero-current force at around 50 N. The "ss420" line represents the peak power of the initial design if the core was ferromagnetic stainless-steel instead of NdFeB.

Table 1. Electromagnet specifications for the initial design used in the parameter sweep, the chosen design, and the manufactured electromagnet.

	C (mm)	H (mm)	R (mm)	T (mm)	L (mm)	core	wire (awg)	N (turns)	M_{mag} (kg)	F_0 (N)	$F_{p,max}$ (N)	P_{max} (W)
design range	20-40	5-30	30-60	1-6	±5	n30-n50	15-24	-	-	-	-	-
initial	25	15.0	50.0	3.0	2.5	n42	18	348	1.27	53.0	88.1	201
chosen	28	9.4	50.6	4.3	2.8	n42	18	198	1.05	50.6	86.3	201
manufactured	28	9.5	49.1	5.5	2.2	n42	19	228	1.02	51.8	86.1	228

B. Implant design

Our dissections showed surgical feasibility of placing a ferromagnetic implant in the distal residual femur. Aligning our initial implant design priorities with our observations during the dissections, we converged on an ovular implant with a 100 mm major axis and 70 mm minor axis (**Fig. 3a)**. The surgeon members of our team developed an operative approach whereby the implant will be covered by a full thickness hamstring flap (*biceps femoris* and *semimembranosus*) sutured orthogonally to a transverse adductor myodesis (**Fig. 3b**). This allows the implant to be fully covered in muscle, without creating issues for closure of the skin envelope. The tissue thickness below the implant was measured to be between 12.5 and 17.5 mm. A gap distance of 17.5 mm was chosen for modeling the system.

C. Electromagnet design

1-dimensional sweeps of each design parameter showed that every parameter influenced system performance, with lip height having the least overall impact (**Fig. 4**). The peak power (P_{max}) required to produce $F_{p,max}$ decreased exponentially as core radius, coil/core height, coil radius, and shell thickness increased. Higher NdFeB grades also substantially decreased P_{max}, albeit in a more linear fashion. Lip height decreased P_{max} as well, but the effect was relatively small (60 W range of P_{max} compared to 1200 W range for coil/core height). The mass of the electromagnet (M_{mag}) increased the most as a function of coil/core height and coil radius, with shell thickness also increasing M_{mag} to a lesser degree. Core material, core radius, and lip height had little effect on M_{mag}. Zero-current force (F_0) was most affected by the core radius and coil/core height (94 N and 62 N ranges, respectively). Increases in NdFeB grade, coil radius, and shell thickness also increased F_0 slightly (< 25 N ranges). The design parameters of the initial design used for the sweep and the chosen design are listed in Table 1.

In the context of the chosen design geometry, higher battery voltages resulted in higher forces for all wire sizes (**Fig. 5a**). For an electromagnet that was powered by a 48 V battery, the force at positive battery voltage was greater than the peak pulloff force for all but the smallest wire size (24 awg). At negative battery voltages (current in the coils producing a field that opposes that of the permanent magnet core), force minima across wire sizes were observed at 16, 18, and 19 awg for -24, -36, and -48 V, respectively (**Fig. 5b**). The values of all minima were below the desired 10 N doffing force (F_{doff}). The electromagnet current at positive battery voltage decreased as wire size decreased (higher awg), with a max current of less

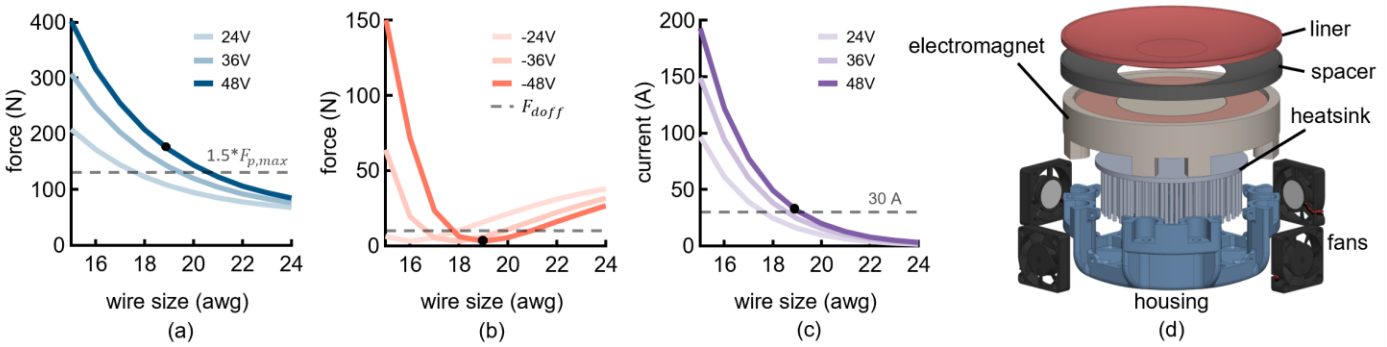

Figure 5. Design considerations for the physical electromagnet. (a) Attractive force generated by the magnet at a 17.5 mm gap distance, while applying positive battery voltage (the field of the electromagnet coil adds to that of the permanent magnet core), as a function of wire size. This represents the condition of maximum possible force production. Dashed line denotes the desired factor of safety above the peak pulloff force for this electromagnet mass. (b) Attractive force generated by the magnet at negative battery voltage (the field of the electromagnet coil opposes that of the permanent magnet core). Dashed line denotes the desired system force during doffing, and the marker indicates the minimum for a 48 V system. (c) Electromagnet current at max battery voltage. Dashed line denotes the 30 A peak current limit of typical prosthetic power systems, and the marker indicates a 48 V, 19 awg system. (d) The completed system incorporates a spacer/liner between the electromagnet and the skin, along with a heatsink, housing, and fans.

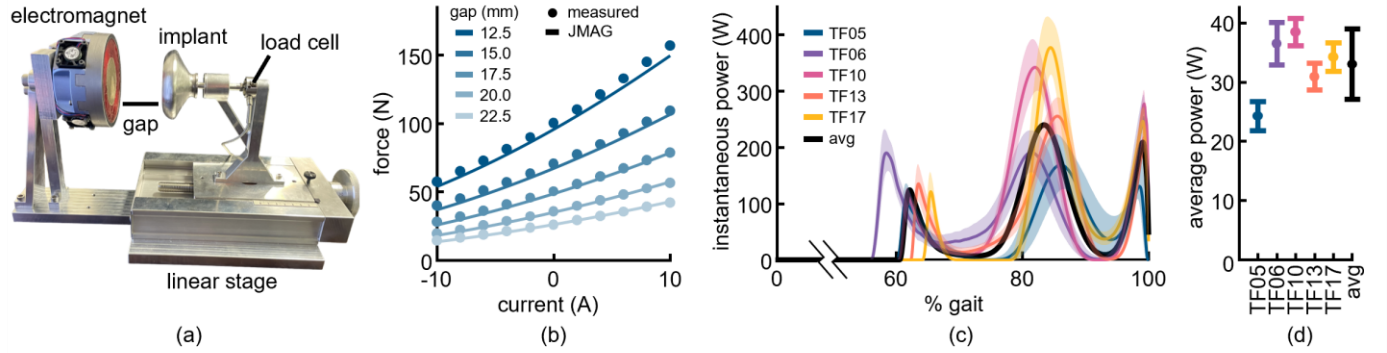

Figure 6. Feasibility of power requirements for electromagnetic suspension. (a) Testbench setup with the stationary electromagnet and the implant mounted to a linear stage. An in-line load cell measures the force on the implant. (b) Measured (dots) and JMAG-predicted (lines) forces for varying currents and gap distances. (c) Instantaneous power over the gait cycle for five persons with transfemoral amputation. Power was calculated from each subject's average pulloff force, and the inter-subject average of these averages (black line). The system would be "off" during stance phase (0 W). (d) Average power during gait for each subject and the inter-subject average force profile. The inter-subject average force profile would require around 33 W of average power. Shaded regions and error bars show ±1 st. dev.

than the desired 30 A occurring for wire sizes less than or equal to 18 awg for 24 V and 19 awg for 36 and 48 V (**Fig. 5c**). Based on these results, the combination of a 48 V battery system and 19 awg wire was chosen. This would produce a maximum force of 171 N at 48 V (safety factor of 2 with respect to $F_{p,max}$), a minimum force of 3.1 N at -48 V, and max current of 30 A. The final manufactured design considering integer wire layers and manufacturing clearances is detailed in **Table 1**. The additional components of the complete system are shown in **Fig. 5d**.

D. Power feasibility

Testbench experiments (**Fig. 6a**) showed agreement between the measured and simulated forces produced by the electromagnet as a function of gap distance and electromagnet current, with a root-mean-square percentage error of 4.2% (**Fig. 6b**). The JMAG model systematically underpredicted attractive force. Simulations of the attachment system as manufactured showed that the peak power during gait for the inter-subject average loading profile was 228 W but was as high as 343 W for one subject (**Fig. 6c**). In all subjects, the electromagnet was powered "off" or at low power for most of the gait cycle except for three peaks during swing; as such, the inter-subject average power during gait was 33±5.9 W (**Fig. 6d**).

E. Thermal feasibility

Heating of the electromagnet during continuous walking was evaluated on the benchtop using the simplified power profile seen in **Fig. 7a**. The actual current applied to the electromagnet closely tracked this desired curve. Two setups (**Fig. 7b**) of the testbench were used to first measure shell and housing temperatures, and then liner temperatures in two separate trials. Thermal imaging showed an uneven heat distribution between components, with the shell being hotter than the housing (**Fig. 7c**, top), and an outer ring of the liner being hotter than the center (**Fig. 7c**, bottom). Active cooling consistently reduced the temperatures of all components (**Fig. 7d**). At the surface of the liner, which would be in contact with the limb, the temperature increased a maximum of 0.5°C and 2.3°C from ambient after 100 and 200 steps, respectively. These increases were similar between active and passive cooling. After 500 and 1000 steps in the active cooling case, the liner temperature had increased by 8.6°C and 15.4°C.

F. Cost function analysis

As a function of the weights C_f, C_m, and C_0, the design parameters increased for increasing C_f, and decreased for

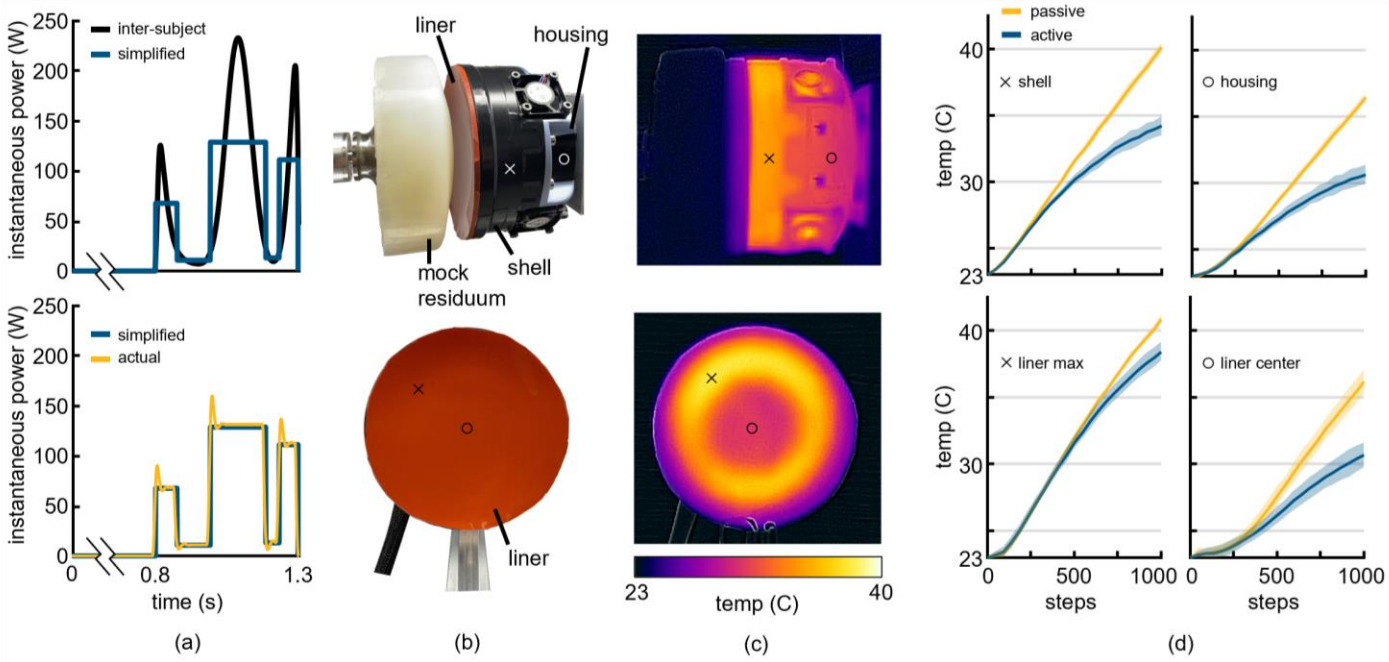

Figure 7. Thermal heating of the electromagnet during benchtop simulations of continuous gait. (a) Power profiles used to simulate one stride. The inter-subject instantaneous power curve was simplified into 6 discrete intervals, where the power in each interval was set at the average power of the inter-subject profile for that interval. (b) Testbench setups for each round of testing. Temperatures of the shell (x) and housing (o) were measured with the mock residuum in contact with the liner (top image). In a separate trial, the max (x) and center (o) temperatures of the liner were measured by removing the mock limb (bottom image). (c) Thermal images of the actively cooled electromagnet after 1000 simulated steps. (d) Temperatures of the shell, housing, and liner for passive and active cooling of the electromagnet. Shaded regions show ±1 st. dev.

increasing C_m and C_0 (**Fig. 8a,b**). A notable exception was the core radius (C) as a function of C_m. As C_m increases starting from low values, core radius starts to decrease until a critical value of C_m is reached. At this point, the core radius increases for larger values of C_m (**Fig. 8b**).

The three "optimal" designs for prioritizing each of the cost weights illustrate how the cost weights influence the resulting electromagnet (**Fig. 8c**), and highlight the tradeoffs between magnet mass, force production, and power required for doffing. Prioritizing C_f resulted in a large electromagnet that could produce high forces; however, doffing would require high powers (1.9 kW). Prioritizing C_m created a small, light magnet that could not produce as much force, but required less power to doff. Prioritizing C_0 resulted in the smallest electromagnet with the smallest core that could not produce high forces.

IV. Discussion

In this manuscript, we showed the feasibility of a new prosthetic attachment paradigm utilizing magnetic attraction between a bone-anchored ferromagnetic implant and an external electromagnet. We established a design framework for developing this system at any amputation level, and evaluated this framework in the context of an above-knee amputation. This framework entails estimating the socket pulloff force through biomechanical analysis, designing the implant based on cadaveric dissections, analyzing electromagnet geometry through electromagnetic simulations of performance, and validating the resulting system on the benchtop. We also presented a cost function by which this system could be optimized, and explored implications of prioritizing different parts of that cost function.

The socket forces required to attach a knee-ankle-foot prosthesis during the stance phase of gait were observed to vary widely between subjects. Interestingly, this variability was not observed during the swing phase, with suspension loads across subjects having similar timing and magnitude (**Fig. 2a**). These common pulloff force profiles may be due to the same prosthetic limb being modeled for each subject, such that similar swing phase kinematics of the leg would produce similar pulloff forces at the socket. Similarity in these pulloff-force profiles would allow a single system to generalize across many people, which would be advantageous for developing prosthetic attachment systems. It appears from our analysis that if there are large variations in pulloff force between subjects, these variations would be directly tied to mass of the prosthesis in a way that should be easily predictable. Because the mass of the modeled prosthesis was on the high end of robotic research prostheses, which are much heavier than commercial devices [1] used by the subjects in the Hood et al. dataset [43], our analyses represent an upper bound of the pulloff forces that we would expect during level-ground walking. Deviations from our modeled socket mass, which will change from person-to-person as a function of limb geometry, could also affect pulloff force, but would do so in a linear manner as seen in Fig. 2c.

One limitation of using cadaveric models in the implant design procedure is that the specimens may not be representative of the patient population, nor of the atrophic changes that occur in a limb after amputation. These specimens are also surgically "pristine", which cannot fully capture the real-time surgical decision-making of how a residuum should be constructed based on tissue availability and health [47]. All these factors, which are difficult to generalize across patients, could affect the gap distance between the implant and the skin.

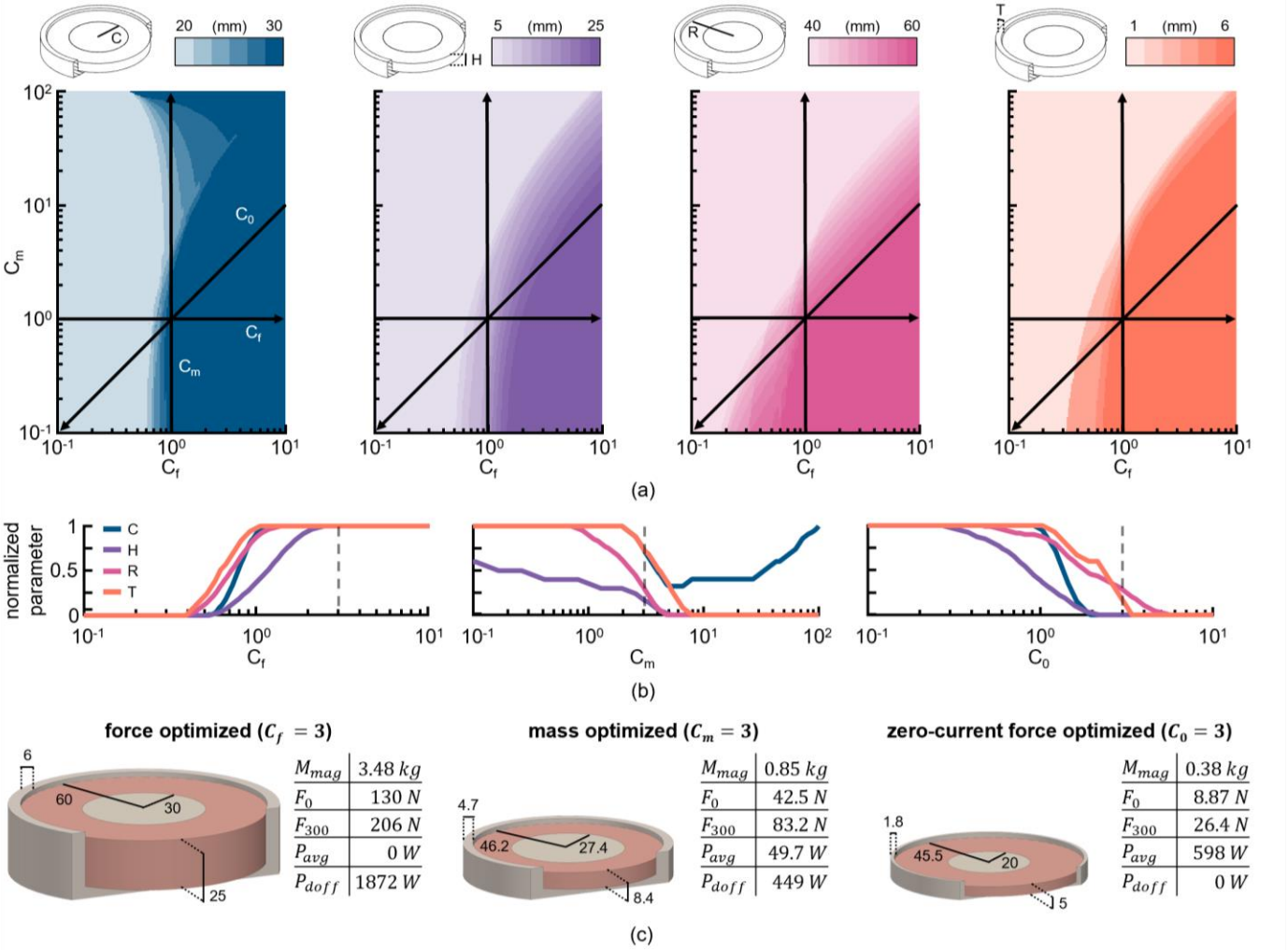

force optimized ($C_f = 3$)	
M_{mag}	3.48 kg
F_0	130 N
F_{300}	206 N
P_{avg}	0 W
P_{doff}	1872 W

mass optimized ($C_m = 3$)	
M_{mag}	0.85 kg
F_0	42.5 N
F_{300}	83.2 N
P_{avg}	49.7 W
P_{doff}	449 W

zero-current force optimized ($C_0 = 3$)	
M_{mag}	0.38 kg
F_0	8.87 N
F_{300}	26.4 N
P_{avg}	598 W
P_{doff}	0 W

Figure 8. Analysis of a cost function for optimizing the electromagnet geometry. (a) Design parameters of the "optimal" (minimal cost) design as a function of the cost weights for force (C_f) and mass (C_m). (b) Changes in the design parameters for independent changes in one cost weight while the other two are set to unity. These depict the cross section of the surfaces along each of the three arrows in part a. (C) Simulated performance of three optimal designs for cost function weights that prioritize force, mass, and zero-current force. Performance metrics are electromagnet mass (M_{mag}), zero-current force (F_0), force at 300 W (F_{300}), average power during gait (P_{avg}), and power required to reach the desired 10 N force for doffing (P_{doff}). The locations of these designs in the plots of part b are denoted by the vertical dashed lines.

Fortunately, the limb tissues used for coverage are both mechanically compliant and surgically malleable, and the attractive force between the electromagnet and implant is controllable, such that it should be feasible to accommodate different tissue thicknesses. The size and shape of the implant were primarily determined by the anatomical constraints of the residual limb; while we do expect that the residual limb envelope will indeed dictate overall sizing of the implant, future work will revisit the specific design to optimize the implant's magnetic properties or mass within these size constraints.

By sweeping different electromagnet designs, we found that a permanent magnet core instead of a traditional ferromagnetic core was a crucial design element for the electromagnet. As seen in **Fig. 4**, the power required to reach the peak pulloff force for an electromagnet with a ferromagnetic SS400 core (778 W) was much greater than those with NdFeB cores. This massive peak power is due to force being proportional to current, but power being proportional to current squared. Implementing a permanent magnet core greatly reduced the power requirements: the core produces most of the baseline force related to suspending the prosthesis mass, such that the coil is only actively controlled during the short-duration dynamic forces in swing (**Fig. 6c**). We also found that the ferromagnetic shell surrounding the coil and core was key to the system's feasibility. Even though the shell adds "passive mass" (e.g. mass that is not producing a magnetic field), the shell material *concentrates* and *focuses* the magnetic field above the electromagnet such that higher attractive forces are achieved for the same power. The importance of the shell was apparent from the results of the parameter sweep (**Fig. 4**): increasing the shell thickness resulted in similar reductions in P_{max} to increasing the coil/core height and coil radius, but had much less impact on mass than either of these two parameters.

Benchtop characterization of the manufactured system successfully validated the design framework's ability to predict system performance. This gives us confidence in the potential for this simulation framework to serve as the basis for application-specific magnet optimization in the future. Based on these benchtop measurements, our estimates of the power required during gait are well within the capabilities of current

power electronics found on powered prostheses [1], [42]. The 33 W average power could be supplied by a 200g battery (two RDQ 6s 720mAh LiHV batteries in series), which would provide a full day of walking (~5000 steps [48]) on a single charge. Note that this adds only 10% to the expected mass of the electromagnet-socket system. To reduce the effect of this mass, batteries would be placed as proximally as possible.

Heating was of primary concern during our initial conception of the electromagnetic attachment architecture; fortunately, benchtop thermal performance of the manufactured electromagnet was promising. Because 96% percent of bouts during daily living tend to be 200 steps or less [49], temperature at the skin under typical use would not increase more than 2.3℃, regardless of active or passive cooling (**Fig. 7d**). This increase is slightly greater than those measured in conventional sockets during activity [50]–[52]; however, with an electromagnetic attachment system, the socket could be breathable such that these hotspots remain localized. This could potentially decrease overall sweating of the limb and reduce skin irritation. For longer bouts or individuals with higher activity levels, however, heating is the primary barrier to feasibility. While the 15.4℃ temperature increase after 1000 steps brought the liner (38.4℃) to just over body core temperature (37.2℃) and would not cause burns, it is notable that long duration exposure (4-5 hours) to temperatures >43℃ can lead to tissue damage [53]. This calls for refinement of the design, which we plan to achieve via optimization with an emphasis on reducing power. For instance, one change to improve the design is replacing the n42 NdFeB grade permanent magnet core with a stronger n52 grade. This will reduce the size of the core for the same zero-current force, allowing for more coil turns in the same electromagnet size.

Analysis of the cost function we proposed for the optimization of the electromagnet revealed interesting insights into the impact of each design parameter. Most apparent was the abrupt change in the core radius as $C_m$was increased (**Fig. 8b**). At high values of C_m, the three other parameters are driven to the minimum bound. Around the point that these parameters reach their respective minima, the core radius reverses course and starts increasing. One explanation is that the mass of the electromagnet is more effectively utilized by a stronger permanent magnet core than by the coils. This idea is supported by observations from the first parameter sweep (**Fig. 4**), which showed that increasing the core radius greatly increased the electromagnet force (lower peak power and higher zero-current force), with minimal change in mass. For cost functions not heavily weighting mass, this effect is diminished by the penalty from the higher zero-current force. As a whole, the large variations in electromagnet geometry as a function of the cost weights showed that this cost function will be useful for tuning the electromagnet design based on design priorities such as reducing the power requirements of the attachment system.

Because the implant is a soft ferromagnet, rather than a permanent magnet, it is only possible to produce an attractive force between the implant and the external electromagnet. The choice of a soft ferromagnetic implant was made to limit possible interactions between a strong magnetic field within the leg and the environment. When the ferromagnetic implant is not in the presence of a magnetic field (e.g. when the socket is not being worn), the residuum is not attracted to the environment. In the presence of the external electromagnet, the ferromagnetic implant material serves as a shield for the region proximal to the implant, and the ferromagnetic shell of the electromagnet shields the region distal and adjacent to the electromagnet, such that the field remains concentrated in the space between the implant and the electromagnet. Despite the inability to provide *repulsion*, the attachment system still has potential to provide substantial benefit during the stance phase. For instance, by eliminating pistoning, it may be possible to mitigate the shock loads that occur on the residual bone during heel strike, which will substantially reduce peak stance-phase stresses on the residuum. In addition, the large distal surface area of the implant may help distribute compressive loads and avoid stress concentrations [40], [41]. The oblique geometry of the implant may also prevent rotation of the prosthetic socket with respect to the residual femur, to stabilize the prosthesis in the context of twisting motions. We expect these benefits to hold even with the added compressive force exerted on the residual limb during stance by the permanent magnet core when the electromagnet is powered off, especially given that the magnitude of this passive force is much lower than weightbearing forces.

Although the electromagnetic socket will likely be heavier than a conventional socket, the shift from soft-tissue suspension to bony suspension is expected to help compensate for the added mass. We recognize the importance of mass in clinical viability of prosthetic devices; many patients abandon their prostheses because they are too heavy, or opt for passive devices with reduced functionality simply because they weigh less than robotic alternatives [54]–[56]. This is primarily a perception issue: robotic prostheses are typically comparable in weight to the *biological* limb, but are perceived as too heavy when used in conjunction with a socket [15], [54], [57], [58]. This distorted perception happens in large part because the prosthesis is suspended from soft tissue, whereas the biological limb is suspended from bone. Bony suspension can increase tolerance of prosthetic mass, as evidenced by improvements in satisfaction, embodiment, and time of use when patients with OI are prescribed the same prosthetic devices that are described as “too heavy” when used with conventional sockets [28], [30], [38], [59]. In light of these considerations, although we still sought to minimize the system’s mass, we do not believe that perceived weight would limit the adoption of this system.

Another potential clinical challenge is that, by its nature, the ferromagnetic implant will not be compatible with magnetic resonance imaging (MRI). This is a non-trivial concern because MRI is the dominant non-radiating medical imaging modality. However, there are many existing clinical devices, such as cochlear implants [60], [61] and cardiac pacemakers [62], [63], for which lack of MRI compatibility is an acceptable compromise. One important use of MRI in orthopaedics is in identifying periprosthetic infection and osteomyelitis, which could pose complication risks for the implant (although the risk should be much lower for this implant than for percutaneous OI). In current clinical practice, bone infection is diagnosed through a multimodal approach that combines physical examination, bacteriological sampling, and imaging. MRI is only one of several imaging techniques used in diagnosis; alternatives include plain x-ray, computerized tomography, and nuclear medicine [64]. A drawback of using these other techniques is exposure to radiation. However, considering the

potential benefits of electromagnetic suspension and the fact that OI patients accept chronic infection risk for similar benefits, it seems plausible that the value of improved prosthetic fit is worth a compromise in MRI compatibility.

This work demonstrated the theoretical feasibility of electromagnetic attachment of prosthetic limbs. In future research, we will optimize the electromagnet and implant designs using the framework presented in this paper, and extend this framework to other levels of amputation. Further testing will be done as we develop a control architecture to stabilize this system, which is essentially a large-gap electromagnetic force control problem complicated by nonlinear soft-tissue interactions. In evaluating the system's effectiveness, it must be compared to conventional sockets using metrics of clinical relevance, such as overall tissue deformation during gait.

V. Conclusion

Electromagnetic attachment of prosthetic limbs has the potential to increase comfort, improve residual limb health, and provide additional function by suspending the prosthesis directly from bone without creating a chronic wound. Our design framework can be used to optimize electromagnetic suspension systems for specific amputation levels. We validated this system in designing a device for transfemoral amputation, and showed that this device would be feasible with the power electronics currently used in powered knee-ankle-foot prostheses, and would result in minimal heating of the residual limb during short walking bouts (< 200 steps). In future work, we will optimize this system to reduce heating during longer bouts and test the physical system under dynamic loads.

Acknowledgment

This work was funded by the National Science Foundation Graduate Research Fellowship Program, by the U.S. Department of Defense congressionally directed medical research programs, and by the National Science Foundation Disability and Rehabilitation Engineering program. T. R. Clites, N. M. Bernthal, A.I. Stavrakis, H. Warren, and W. Flanagan are listed as inventors on a patent related to this work. The authors would like to thank Gabriel Olin for help with the OpenSim pipeline, Shilpa Rao for assistance with electronics, and Vehan Doshi for data processing contributions.

References

[1] M. Tran, L. Gabert, S. Hood, and T. Lenzi, "A Lightweight Robotic Leg Prosthesis Replicating the Biomechanics of the Knee, Ankle, and Toe Joint," *Sci. Robot.*, pp. 1–18, 2022.

[2] T. R. Clites *et al.*, "Proprioception from a neurally controlled lower-extremity prosthesis," *Sci. Transl. Med.*, vol. 10, no. 443, 2018.

[3] A. S. Voloshina and S. H. Collins, *Lower limb active prosthetic systems-overview*. INC, 2019.

[4] T. A. Kuiken *et al.*, "Targeted muscle reinnervation for real-time myoelectric control of multifunction artificial arms," *Jama*, vol. 301, no. 6, pp. 619–628, 2009.

[5] H. M. Herr and A. M. Grabowski, "Bionic ankle-foot prosthesis normalizes walking gait for persons with leg amputation," *Proc. R. Soc. B Biol. Sci.*, vol. 279, no. 1728, pp. 457–464, 2012.

[6] D. W. Tan, M. A. Schiefer, M. W. Keith, J. R. Anderson, J. Tyler, and D. J. Tyler, "A neural interface provides long-term stable natural touch perception," *Sci. Transl. Med.*, vol. 6, no. 257, 2014.

[7] S. Raspopovic *et al.*, "Bioengineering: Restoring natural sensory feedback in real-time bidirectional hand prostheses," *Sci. Transl. Med.*, vol. 6, no. 222, 2014.

[8] T. S. Davis *et al.*, "Restoring motor control and sensory feedback in people with upper extremity amputations using arrays of 96 microelectrodes implanted in the median and ulnar nerves," *J. Neural Eng.*, vol. 13, no. 3, 2016.

[9] M. K. Shepherd and E. J. Rouse, "Design of a quasi-passive ankle-foot prosthesis with biomimetic, variable stiffness," *Proc. - IEEE Int. Conf. Robot. Autom.*, pp. 6672–6678, 2017.

[10] R. Gehlhar, M. Tucker, A. J. Young, and A. D. Ames, "A review of current state-of-the-art control methods for lower-limb powered prostheses," *Annu. Rev. Control*, no. December 2022, 2023.

[11] L. J. Hargrove *et al.*, "Intuitive control of a powered prosthetic leg during ambulation: A randomized clinical trial," *JAMA - J. Am. Med. Assoc.*, vol. 313, no. 22, pp. 2244–2252, 2015.

[12] T. R. Dillingham, L. E. Pezzin, E. J. MacKenzie, and A. R. Burgess, "Use and satisfaction with prosthetic devices among persons with trauma-related amputations: a long-term outcome study.," *Am. J. Phys. Med. Rehabil.*, vol. 80, no. 8, pp. 563–571, Aug. 2001.

[13] L. E. Pezzin, T. R. Dillingham, E. J. MacKenzie, P. Ephraim, and P. Rossbach, "Use and satisfaction with prosthetic limb devices and related services," *Arch. Phys. Med. Rehabil.*, vol. 85, no. 5, pp. 723–729, 2004.

[14] K. Hagberg and R. Brånemark, "Consequences of non-vascular trans-femoral amputation: A survey of quality of life, prosthetic use and problems," *Prosthet. Orthot. Int.*, vol. 25, no. 3, pp. 186–194, 2001.

[15] E. Biddiss and T. Chau, "Upper-limb prosthetics: Critical factors in device abandonment," *Am. J. Phys. Med. Rehabil.*, vol. 86, no. 12, pp. 977–987, 2007.

[16] S. Salminger *et al.*, "Current rates of prosthetic usage in upper-limb amputees–have innovations had an impact on device acceptance?," *Disabil. Rehabil.*, vol. 44, no. 14, pp. 3708–3713, 2022.

[17] E. E. Haggstrom, E. Hansson, and K. Hagberg, "Comparison of prosthetic costs and service between osseointegrated and conventional suspended transfemoral prostheses," *Prosthet. Orthot. Int.*, vol. 37, no. 2, pp. 152–160, 2013.

[18] A. Dobson, A. El-Gamil, M. Shimer, and J. E. Davanzo, "Economic value of prosthetic services among medicare beneficiaries: A claims-based retrospective cohort study," *Mil. Med.*, vol. 181, no. 2, pp. 18–24, 2016.

[19] C. P. F. Pasquina, A. J. Carvalho, and T. P. Sheehan, "Ethics in rehabilitation: Access to prosthetics and quality care following amputation," *AMA J. Ethics*, vol. 17, no. 6, pp. 535–546, 2015.

[20] A. Eshraghi, N. A. A. Osman, H. Gholizadeh, M. Karimi, and S. Ali, "Pistoning assessment in lower limb prosthetic sockets," *Prosthet. Orthot. Int.*, vol. 36, no. 1, pp. 15–24, 2012.

[21] K. Ziegler-Graham, E. J. MacKenzie, P. L. Ephraim, T. G. Travison, and R. Brookmeyer, "Estimating the Prevalence of Limb Loss in the United States: 2005 to 2050," *Arch. Phys. Med. Rehabil.*, vol. 89, no. 3, pp. 422–429, 2008.

[22] L. Paternò, M. Ibrahimi, E. Gruppioni, A. Menciassi, and L. Ricotti, "Sockets for limb prostheses: A review of existing technologies and open challenges," *IEEE Trans. Biomed. Eng.*, vol. 65, no. 9, pp. 1996–2010, 2018.

[23] H. E. Meulenbelt, J. H. Geertzen, M. F. Jonkman, and P. U. Dijkstra, "Determinants of Skin Problems of the Stump in Lower-Limb

Amputees," *Arch. Phys. Med. Rehabil.*, vol. 90, no. 1, pp. 74–81, 2009.

[24] J. T. Kahle and M. J. Jason Highsmith, "Transfemoral sockets with vacuum-assisted suspension comparison of hip kinematics, socket position, contact pressure, and preference: Ischial containment versus brimless," *J. Rehabil. Res. Dev.*, vol. 50, no. 9, pp. 1241–1252, 2013.

[25] R. D. Alley, T. W. Williams, M. J. Albuquerque, and D. E. Altobelli, "Prosthetic sockets stabilized by alternating areas of tissue compression and release," *J. Rehabil. Res. Dev.*, vol. 48, no. 6, pp. 679–696, 2011.

[26] R. P. Brånemark, K. Hagberg, K. Kulbacka-Ortiz, Ö. Berlin, and B. Rydevik, "Osseointegrated Percutaneous Prosthetic System for the Treatment of Patients with Transfemoral Amputation: A Prospective Five-year Follow-up of Patient-reported Outcomes and Complications," *J. Am. Acad. Orthop. Surg.*, vol. 27, no. 16, pp. E743–E751, 2019.

[27] J. S. Hoellwarth, K. Tetsworth, S. R. Rozbruch, M. B. Handal, A. Coughlan, and M. Al Muderis, "Osseointegration for Amputees," *JBJS Rev.*, vol. 8, no. 3, pp. e0043–e0043, 2020.

[28] B. W. Hoyt, S. A. Walsh, and J. A. Forsberg, "Osseointegrated prostheses for the rehabilitation of amputees (OPRA): results and clinical perspective," *Expert Rev. Med. Devices*, vol. 17, no. 1, pp. 17–25, 2020.

[29] K. Hagberg and R. Brånemark, "One hundred patients treated with osseointegrated transfemoral amputation prostheses - Rehabilitation perspective," *J. Rehabil. Res. Dev.*, vol. 46, no. 3, pp. 331–344, 2009.

[30] D. Juhnke, J. P. Beck, S. Jeyapalina, and H. H. Aschoff, "Fifteen years of experience with Integral-Leg-Prosthesis: Cohort study of Artificial Limb Attachment System," *J. Rehabil. Res. Dev.*, vol. 52, no. 4, pp. 407–420, 2015.

[31] J. Tillander, K. Hagberg, L. Hagberg, and R. Brånemark, "Osseointegrated titanium implants for limb prostheses attachments: infectious complications.," *Clin. Orthop. Relat. Res.*, vol. 468, no. 10, pp. 2781–8, Oct. 2010.

[32] S. Jeyapalina, J. P. Beck, K. N. Bachus, D. L. Williams, and R. D. Bloebaum, "Efficacy of a porous-structured titanium subdermal barrier for preventing infection in percutaneous osseointegrated prostheses," *J. Orthop. Res.*, vol. 30, no. August, pp. 1304–1311, 2012.

[33] D. L. Williams, R. D. Bloebaum, J. P. Beck, and C. A. Petti, "Characterization of bacterial isolates collected from a sheep model of osseointegration," *Curr. Microbiol.*, vol. 61, no. 6, pp. 574–583, 2010.

[34] R. Atallah, R. A. Leijendekkers, T. J. Hoogeboom, and J. P. Frölke, "Complications of bone-anchored prostheses for individuals with an extremity amputation: A systematic review," *PLoS One*, vol. 13, no. 8, pp. 0–3, 2018.

[35] M. B. Zaid, R. J. O'Donnell, B. K. Potter, and J. A. Forsberg, "Orthopaedic Osseointegration: State of the Art," *J. Am. Acad. Orthop. Surg.*, vol. 27, no. 22, pp. E977–E985, 2019.

[36] G. Tsikandylakis, Ö. Berlin, and R. Brånemark, "Implant survival, adverse events, and bone remodeling of osseointegrated percutaneous implants for transhumeral amputees.," *Clin. Orthop. Relat. Res.*, vol. 472, no. 10, pp. 2947–2956, 2014.

[37] J. Tillander, K. Hagberg, L. Hagberg, and R. Brånemark, "Osseointegrated titanium implants for limb prostheses attachments: Infectious complications," *Clin. Orthop. Relat. Res.*, vol. 468, no. 10, pp. 2781–2788, 2010.

[38] K. Hagberg and R. Brånemark, "One hundred patients treated with osseointegrated transfemoral amputation prostheses--rehabilitation perspective.," *J. Rehabil. Res. Dev.*, vol. 46, no. 3, pp. 331–344, 2009.

[39] K. Hagberg, E. Hansson, and R. Brånemark, "Outcome of percutaneous osseointegrated prostheses for patients with unilateral transfemoral amputation at two-year follow-up," *Arch. Phys. Med. Rehabil.*, vol. 95, no. 11, pp. 2120–2127, 2014.

[40] M. Assal *et al.*, "A New Implant for Transfemoral Amputation: Improved Gait and Comfort," *Open J. Orthop.*, vol. 11, no. 06, pp. 199–205, 2021.

[41] L. Guirao, C. B. Samitier, M. Costea, J. M. Camos, M. Majo, and E. Pleguezuelos, "Improvement in walking abilities in transfemoral amputees with a distal weight bearing implant," *Prosthet. Orthot. Int.*, vol. 41, no. 1, pp. 26–32, 2017.

[42] A. F. Azocar, L. M. Mooney, J. F. Duval, A. M. Simon, L. J. Hargrove, and E. J. Rouse, "Design and clinical implementation of an open-source bionic leg," *Nat. Biomed. Eng.*, vol. 4, no. 10, pp. 941–953, 2020.

[43] S. Hood, M. K. Ishmael, A. Gunnell, K. B. Foreman, and T. Lenzi, "A kinematic and kinetic dataset of 18 above-knee amputees walking at various speeds," *Sci. Data*, vol. 7, no. 1, pp. 1–8, 2020.

[44] S. L. Delp *et al.*, "OpenSim: Open-source software to create and analyze dynamic simulations of movement," *IEEE Trans. Biomed. Eng.*, vol. 54, no. 11, pp. 1940–1950, 2007.

[45] R. L. Bona, N. A. Gomeñuka, J. L. L. Storniolo, A. Bonezi, and C. M. Biancardi, "Self-selected walking speed in individuals with transfemoral amputation: recovery, economy and rehabilitation index," *Eur. J. Physiother.*, vol. 22, no. 3, pp. 133–140, 2020.

[46] FLIR, "Use Low-Cost Materials to Increase Target Emissivity," 2015. https://www.flir.com/discover/rd-science/use-low-cost-materials-to-increase-target-emissivity/

[47] H. M. Herr *et al.*, "Reinventing Extremity Amputation in the Era of Functional Limb Restoration," *Ann. Surg.*, vol. Publish Ah, no. Xx, 2020.

[48] M. E. Pepin, K. G. Akers, and S. S. Galen, "Physical activity in individuals with lower extremity amputations: a narrative review," *Phys. Ther. Rev.*, vol. 23, no. 2, pp. 77–87, 2018.

[49] M. S. Orendurff, J. A. Schoen, G. C. Bernatz, A. D. Segal, and G. K. Klute, "How humans walk: Bout duration, steps per bout, and rest duration," *J. Rehabil. Res. Dev.*, vol. 45, no. 7, pp. 1077–1090, 2008.

[50] R. J. Williams, A. Takashima, T. Ogata, and C. Holloway, "A pilot study towards long-term thermal comfort research for lower-limb prosthesis wearers," *Prosthet. Orthot. Int.*, vol. 43, no. 1, pp. 47–54, 2019.

[51] J. T. Peery, W. R. Ledoux, and G. K. Klute, "Residual-limb skin temperature in transtibial sockets," *J. Rehabil. Res. Dev.*, vol. 42, no. 2, pp. 147–154, 2005.

[52] N. Mathur, I. Glesk, and A. Buis, "Skin temperature prediction in lower limb prostheses," *IEEE J. Biomed. Heal. Informatics*, vol. 20, no. 1, pp. 158–165, 2016.

[53] M. W. Dewhirst, L. B. Viglianti, M. Lora-Michiels, P. J. Hoopes, and M. Hanson, "Thermal Dose Requirement for Tissue Effect," *Proc SPIE Int Soc Opt Eng*, vol. 37, no. 3, pp. 338–348, 2003.

[54] R. Gailey *et al.*, "Unilateral lower-limb loss: Prosthetic device use and functional outcomes in servicemembers from Vietnam war and OIF/OEF conflicts," *J. Rehabil. Res. Dev.*, vol. 47, no. 4, pp. 317–332, 2010.

[55] G. H. Kejlaa, "Consumer concerns and the functional value of prostheses to upper limb amputees," *Prosthet. Orthot. Int.*, vol. 17, no. 3, pp. 157–163, 1993.

[56] M. Windrich, M. Grimmer, O. Christ, S. Rinderknecht, and P. Beckerle, "Active lower limb prosthetics: A systematic review of design issues and solutions," *Biomed. Eng. Online*, vol. 15, no. 3, pp. 5–19, 2016.

[57] R. F. Weir, "Design of artificial arms and hands for prosthetic applications," *Stand. Handb. Biomed. Eng. Des.*, pp. 32.1-32.61, 2003.

[58] K. Hagberg, E. Häggström, S. Jönsson, B. Rydevik, and R. Brånemark, "Osseoperception and Osseointegrated Prosthetic Limbs," in *Psychoprosthetics*, P. Gallagher, D. Desmond, and M. MacLachlan, Eds. London: Springer London, 2008, pp. 131–140.

[59] K. Hagberg, R. Brånemark, and O. Hägg, "Questionnaire for Persons with a Transfemoral Amputation (Q-TFA): Initial validity and reliability of a new outcome measure," *J. Rehabil. Res. Dev.*, vol. 41, no. 5, pp. 695–705, 2004.

[60] M. Shew, H. Wichova, J. Lin, L. N. Ledbetter, and H. Staecker, "Magnetic resonance imaging with cochlear implants and auditory brainstem implants: Are we truly practicing MRI safety?," *Laryngoscope*, vol. 129, no. 2, pp. 482–489, 2019.

[61] O. Majdani *et al.*, "Demagnetization of cochlear implants and temperature changes in 3.0T MRI environment," *Otolaryngol. - Head Neck Surg.*, vol. 139, no. 6, pp. 833–839, 2008.

[62] R. Luechinger *et al.*, "In vivo heating of pacemaker leads during magnetic resonance imaging," *Eur. Heart J.*, vol. 26, no. 4, pp. 376–383, 2005.

[63] R. Kalin and M. S. Stanton, "Current clinical issues for MRI scanning of pacemaker and defibrillator patients," *PACE - Pacing Clin. Electrophysiol.*, vol. 28, no. 4, pp. 326–328, 2005.

[64] C. Cyteval and A. Bourdon, "Imaging orthopedic implant infections," *Diagn. Interv. Imaging*, vol. 93, no. 6, pp. 547–557, 2012.